

## Supporting Information

# Kinetically Controlled Synthesis of MOF Nanostructures: Single-Holed Hollow Core-Shell ZnCoS@Co<sub>9</sub>S<sub>8</sub>/NC for Ultra-high Performance Lithium- ion Batteries

Muhammad Kashif Aslam<sup>a</sup>, Syed Shoaib Ahmad Shah<sup>b</sup>, Sha Li<sup>a</sup>, ChangGuo Chen<sup>a\*</sup>

<sup>a</sup> College of Chemistry and Chemical Engineering, Chongqing University,  
Chongqing 401331, P. R. China.

<sup>b</sup> Department of Chemistry, Quaid-i-Azam University Islamabad, 45320, Pakistan.

\*Corresponding authors, E-mail: [cgchen@cqu.edu.cn](mailto:cgchen@cqu.edu.cn) (ChangGuo Chen), [aslam\\_kashif@outlook.com](mailto:aslam_kashif@outlook.com)  
(Muhammad Kashif Aslam)

## Experimental details

### Materials

Zinc nitrate hexahydrate (Zn(NO<sub>3</sub>)<sub>2</sub>·6H<sub>2</sub>O, ≥99.0%), Thioacetamide (C<sub>2</sub>H<sub>5</sub>NS, ≥99.95%) and cobalt nitrate hexahydrate (Co(NO<sub>3</sub>)<sub>2</sub>·6H<sub>2</sub>O, ≥99.0%), 2-Methylimidazole (2-Melm, C<sub>4</sub>H<sub>6</sub>N<sub>2</sub>, ≥99.0%), were all purchased and used without further purification.

**Synthesis of ZIF-67:** In a typical synthesis, two solutions were prepared by dissolving Co(NO<sub>3</sub>)<sub>2</sub>·6H<sub>2</sub>O (291 mg) and 2-methylimidazole (328 mg) in 25 mL of methanol, respectively. Then, the two solutions were mixed rapidly and aged for 24 h at room temperature. The precipitate was washed by ethanol for 4 times before vacuum dried at room temperature overnight.

**Synthesis of time dependent Co-to-Zn ZIF-67/ZIF-8@ZIF-67 core-shell nanoparticles:**

Time dependent ZIF-67@ZIF-8/ZIF67 was prepared as illustrated in Figure S1. Typically,  $\text{Co}(\text{NO}_3)_2 \cdot 6\text{H}_2\text{O}$  (2.5 mmol) was dissolved in 50 mL methanol. 2-methylimidazole (2-mIM 40 mmol) was dissolved in 100 mL methanol. Then the former solution was added to the latter one under vigorous stirring. After 7 minutes, Zn precursor solution of  $\text{Zn}(\text{NO}_3)_2 \cdot 6\text{H}_2\text{O}$  (2.5 mmol) in 50 mL methanol was added. The solution was then left standing for 24 hours. The precipitate was washed by ethanol for refluxing 4 times before vacuum dried at room temperature overnight.

**Synthesis of ZnCoS@CoS yolk-shell structures:** Synthesis of ZnCoS@CoS Yolk-shell is illustrated in Figure 1. Typically synthesized as, 60 mg of ZIF-67@ZIF-8/ZIF67 particles was dispersed in 40 mL of ethanol under ultrasonic, followed by adding 0.25 g of thioacetamide (TAA) and at  $90^\circ\text{C}$  for 15 min. For comparison CoS polyhedrons also fabricated same as above method. Afterwards, the products were harvested by several rinsing-centrifugation cycles.

**Synthesis of single-holed hollow core-shell ZnCoS@Co<sub>9</sub>S<sub>8</sub>/NC:** The ZnCoS@Co<sub>9</sub>S<sub>8</sub>/NC were fabricated by annealing ZnCoS@CoS yolk-shell structures in nitrogen flow for 3h at  $700^\circ\text{C}$  with a ramp rate of  $5^\circ\text{C min}^{-1}$ . For comparison, ZnCo@Co-NC/NC polyhedrons and Co<sub>1-x</sub>S@Co<sub>9</sub>S<sub>8</sub>/NC polyhedrons were also prepared by annealing ZIF-67/ZIF-8@ZIF-67 and CoS polyhedrons under similar conditions, respectively.

**Synthesis of ZnCoS@CoS/NC core-shell:** The ZnCoS@CoS/NC core-shells were fabricated by annealing ZnCoS@CoS yolk-shell structures in nitrogen flow for 3h at  $500^\circ\text{C}$  with a ramp rate of  $5^\circ\text{C min}^{-1}$ .

**Characterization**

The structural characterization and phase purification of as-synthesized materials composite was analyzed by X-ray diffraction (XRD) in the  $2\theta$  range  $10^\circ$ – $90^\circ$  at a scanning rate of  $2^\circ \text{ min}^{-1}$  by an X-ray diffractometer (PANalytical X'Pert powder diffractometer) with a Cu-K $\alpha$  radiation at 40 kV and 40 mA. Nanostructures and morphological investigations were carried out by field emission scanning electron microscope (FESEM) JEOL JSM-7800F. The high-resolution transmission electron microscopy (HRTEM) images were recorded on a JEOL-2100F microscope at 200 kV. The X-ray photoelectron spectroscopy (XPS) was investigated on a Thermo-Fisher scientific instrument using Al K $\alpha$  as the X-ray source. The Brunauer–Emmett–Teller (BET) surface area measurement was carried out at 77.3 K using a Quadrasorb2MP, Quantachrome surface analyzer. Raman spectroscopy was recorded on a LabRAM HR Evolution with 532 nm laser. Thermal stability was checked by thermogravimetric analysis (TGA) using NETZSCH STA 449F thermal analyzer in the temperature range of 30–1200 °C at a heating rate of  $10^\circ \text{ C min}^{-1}$  under N<sub>2</sub> flow.

## **Electrochemical measurements**

Before being assemble the coin-type cells, active materials were dried at  $60^\circ \text{ C}$  for 12h in vacuum to remove solvents (water and NMP molecules). The working electrodes were prepared by a slurry coating procedure. The active materials, conductive agents (carbon black) and polyvinylidene fluoride (PVDF) in a weight ratio of 80:10:10 were dissolved in N-methyl pyrrolidone (NMP) solvent by stirring for overnight. Then the slurry was uniformly coated onto the copper foils and dried at  $60^\circ \text{ C}$  for 12 h in vacuumed oven. After cooling to room temperature, the copper foils were punched into circular discs with a diameter of 14 mm, and the mass load of active materials was determined to be  $\sim 1$ -1.2 mg. The electrodes were assembled into CR2025 coin-type cells with lithium foil as counter electrode, LiPF<sub>6</sub> in EC: DMC (1:1 v/v) as electrolyte,

and Celgard 2400 as separator in an argon filled glove box. During the operation, both the moisture and oxygen levels were controlled below 0.5 ppm. Finally, cyclic voltammetry (CV) was carried out by electrochemical workstation CHI660E at a scan rate of  $0.2 \text{ mV s}^{-1}$  within the range of 0.01-3.0 V. Gavanostatic charge-discharge measurements (GCD) were performed on a LAND battery tester (LANHE CT2001A (Made in China) between 0.01–3.0 V versus  $\text{Li}^+/\text{Li}$ . Electrochemical impedance spectra (EIS) were recorded by electrochemical workstation (LANHE CT2001A (Made in China) in the frequency range from 100 kHz to 0.01 Hz with an AC amplitude of 10 mV.

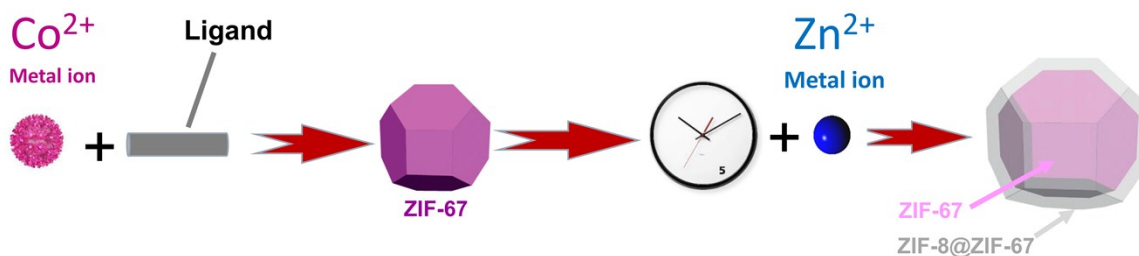


**Figure S1.** General Scheme for the synthesis of kinetic controlled ZIF-67/ZIF-8@ZIF-67.

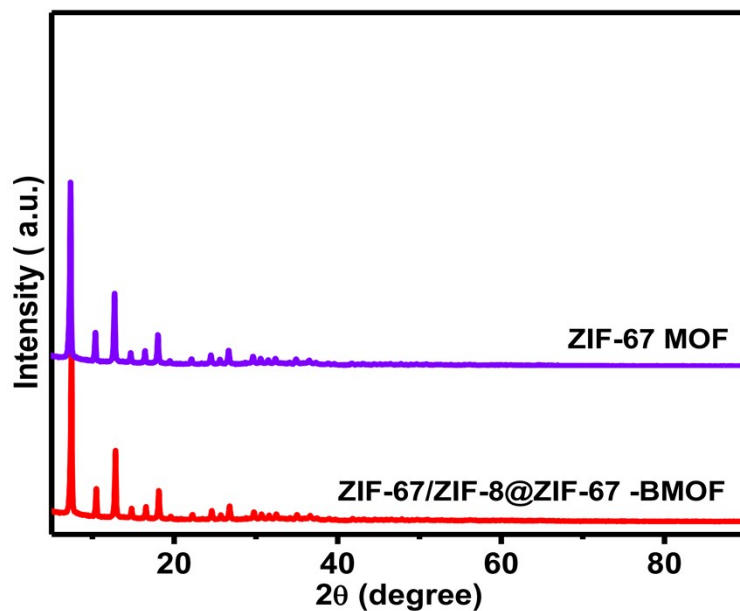


**Figure S2.** XRD patterns of the as-prepared ZIF-67/ZIF-8@ZIF-67 and ZIF-67 MOFs.

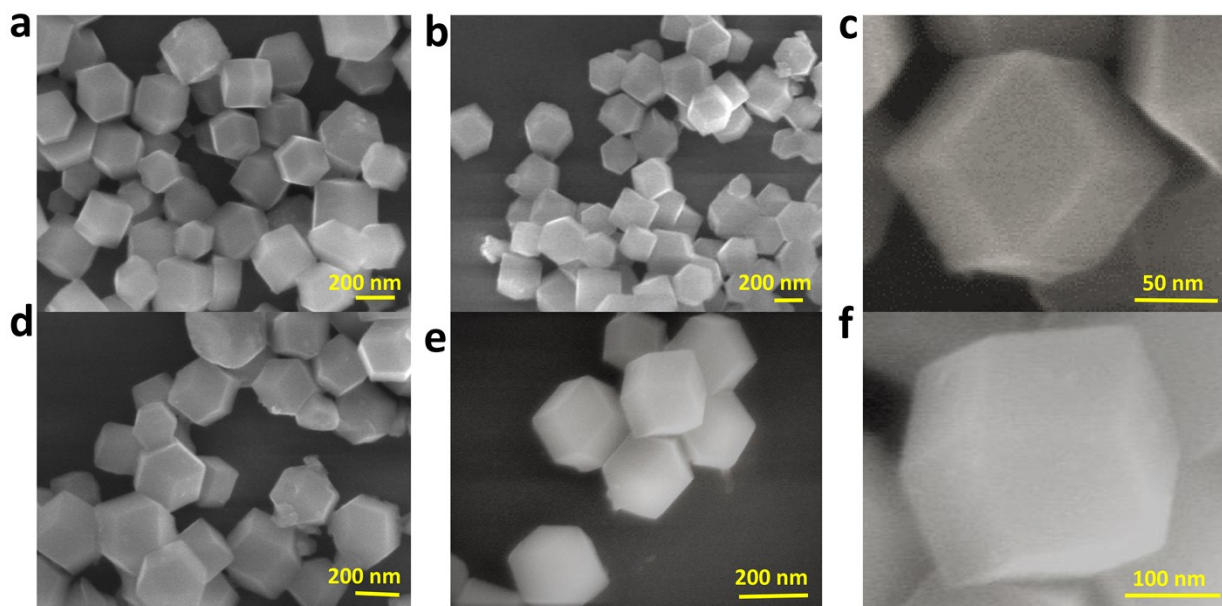


**Figure S3.** FESEM images of ZIF-67 (a-c), and ZIF-67/ZIF-8@ZIF-67 (d-f). FESEM images of both ZIF-67 and ZIF-8@ZIF-67 (Fig. 2S) showing very smooth and surfaced polyhedrons.

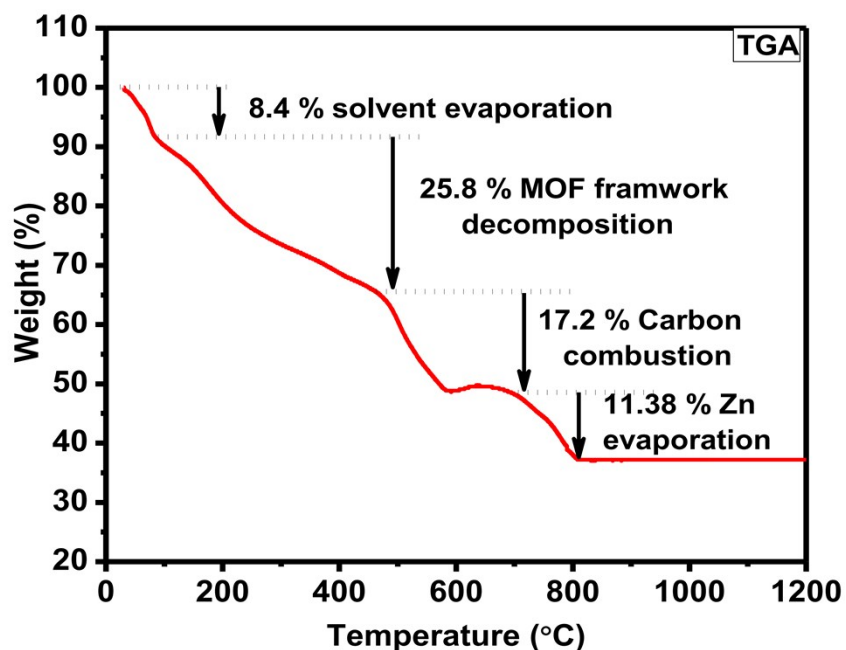


**Figure S4.** TGA curve of sulfidated precursor ZnCoS@CoS/NC yolk-shell.

The exact carbon contents and targeted calcination temperature were investigated by TG analysis as shown in Fig. S6. The Mass loss below 200°C is due to solvent evaporation, and Mass loss up to 480°C is corresponding to decomposition of MOF framework. When temperature increase from 480°C to 580°C then carbon combustion occurred, and after 700°C Zn evaporation started, which is our targeted calcination temperature? The TG analysis curve shows that, Zn evaporation started at 700°C and therefore our targeted calcination temperature was 700°C, because Zn also contributes to the good electrochemical performance due its intrinsic properties, such as lithium alloying reaction.

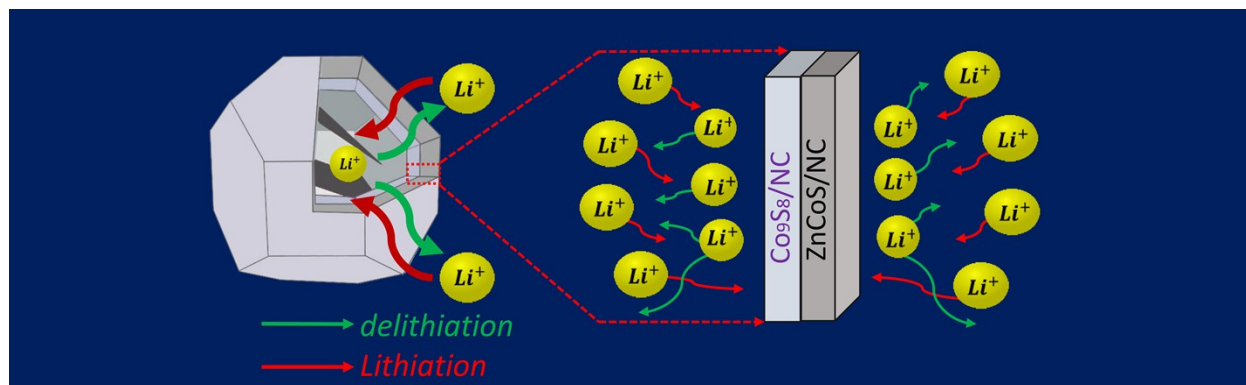


**Figure S5.** Illustration of lithiation and delithiation in single-holed hollow core-shell ZnCoS@Co<sub>9</sub>S<sub>8</sub>/NC electrode.

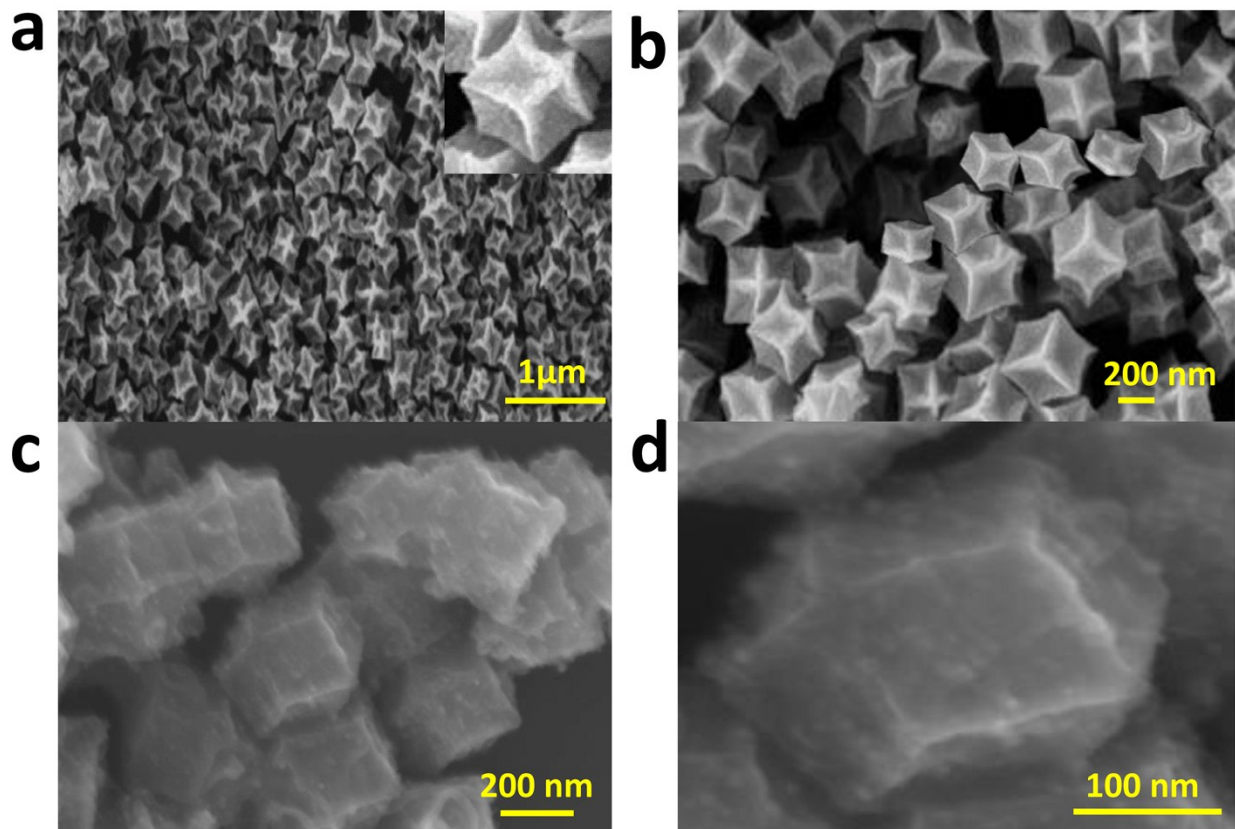


**Figure S6.** FESEM images of Co<sub>1-x</sub>S@Co<sub>9</sub>S<sub>8</sub>/NC (a, b), and ZnCoS@CoS/NC core-shells (c, d).

FESEM images of Co<sub>1-x</sub>S@Co<sub>9</sub>S<sub>8</sub>/NC (Fig. S3 (a, b)) showing contracted polyhedrons, it could be attributed to thin shell of ZIF-67 than ZIF-67/ZIF-8@ZIF-67. For the reasons: (1) during sulfidation S<sup>2-</sup> ions extract Co<sup>2+</sup> from interior to exterior of the polyhedrons and as a result shell of Co<sub>1-x</sub>S@Co<sub>9</sub>S<sub>8</sub>/NC become thin than ZnCoS@CoS/NC core-shells, (2) Co<sub>1-x</sub>S@Co<sub>9</sub>S<sub>8</sub>/NC obtained by calcination at 700°C and ZnCoS@CoS/NC core-shells at 500°C.

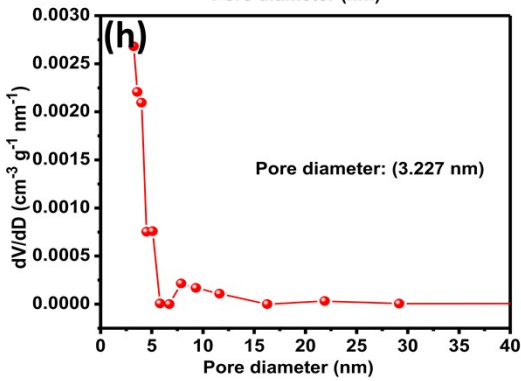
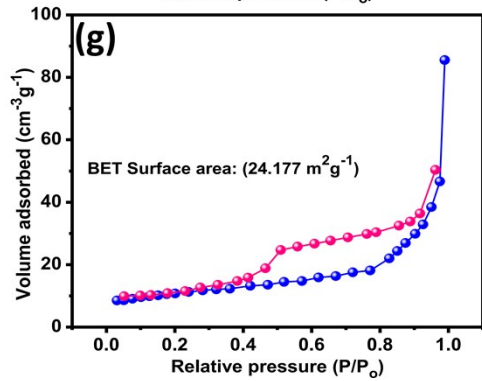
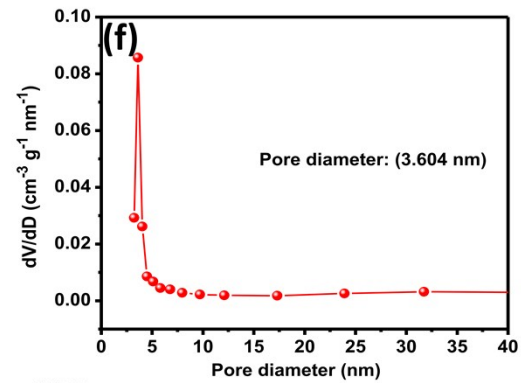
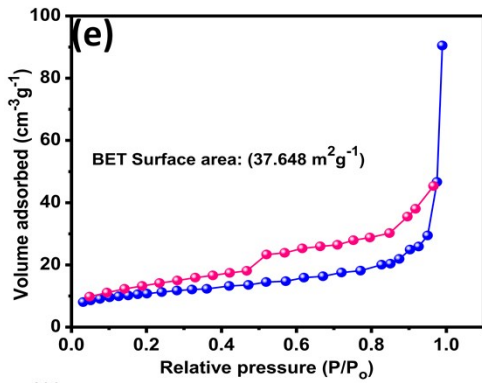
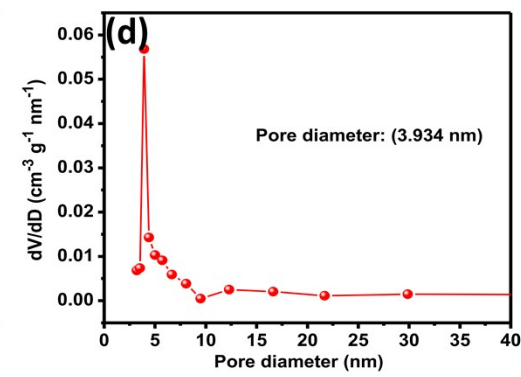
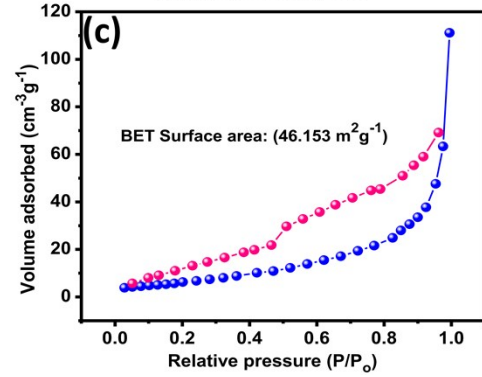
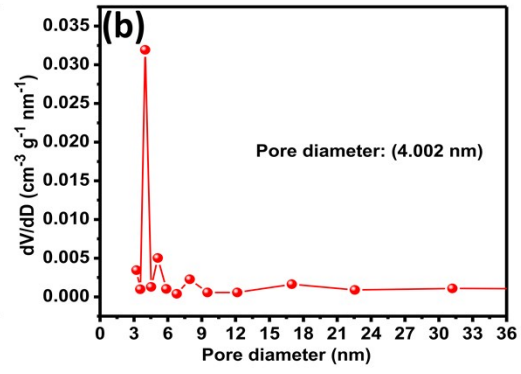
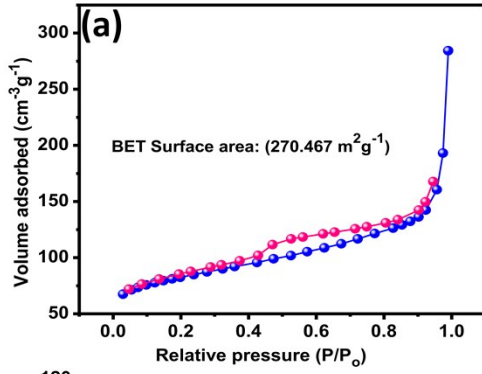


**Figure S7.**  $N_2$  adsorption-desorption and pore diameter of single-holed hollow core-shelled ZnCoS@Co<sub>9</sub>S<sub>8</sub>/NC (a, b), ZnCoS@CoS/NC core-shell (c, d), ZnCo@Co-NC/NC polyhedrons (e, f), and Co<sub>1-x</sub>S@Co<sub>9</sub>S<sub>8</sub>/NC nanocages (g, h).

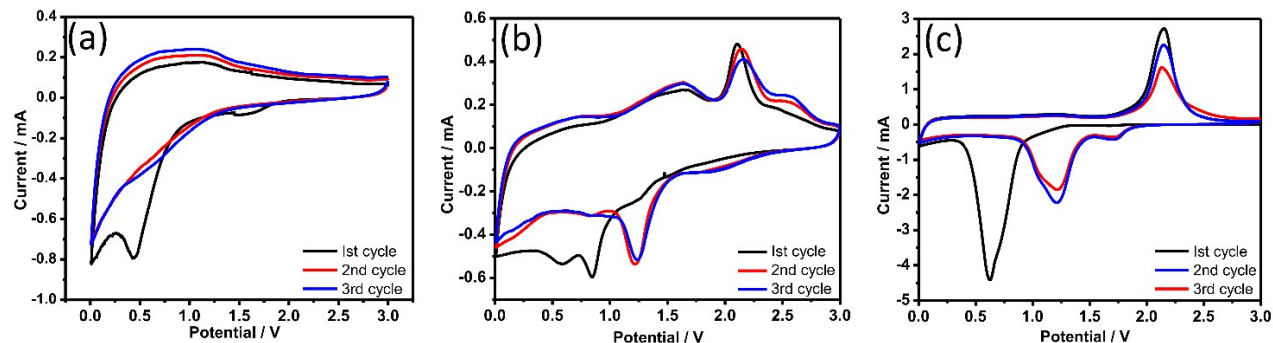


**Figure S8.** CV curves of ZnCo@Co-NC/NC polyhedrons (a), ZnCoS@CoS/NC core-shell (b) and Co<sub>1-x</sub>S@Co<sub>9</sub>S<sub>8</sub>/NC nanocages (c).

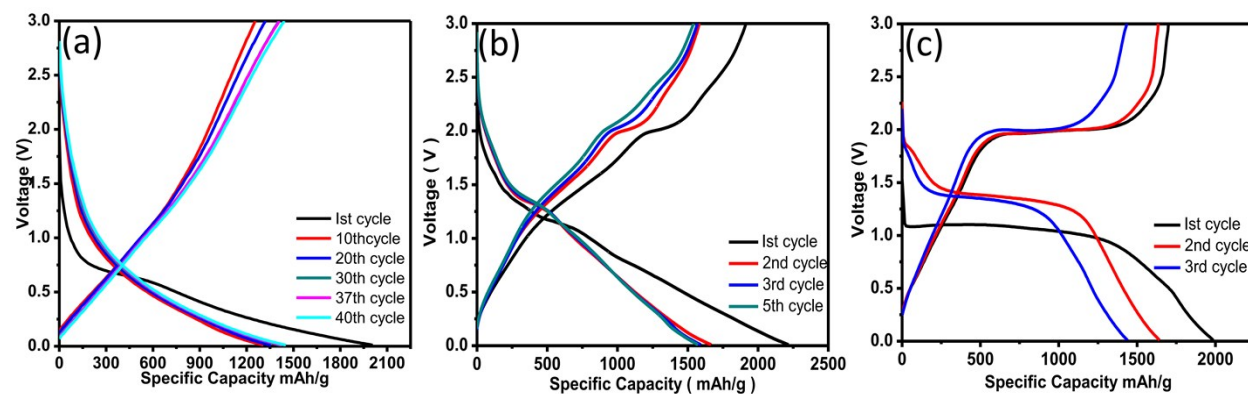


**Figure S9.** Charge-discharge profiles of ZnCo@Co-NC/NC polyhedrons (a), ZnCoS@CoS/NC core-shell (b) and Co<sub>1-x</sub>S@Co<sub>9</sub>S<sub>8</sub>/NC nanocages (c) at a current density of 0.5 A g<sup>-1</sup>.

## Kinetic analysis based on CV results at various scan rates

To explain the high-rate performance, the capacitive contribution of the ZnCoS@Co<sub>9</sub>S<sub>8</sub>/NC electrode are calculated according to the electrochemical response in the cyclic voltammetry (CV) experiment at various sweep rates from 0.1 to 1.0 mV S<sup>-1</sup>. As shown in Figure S11(a), the CV curves for both electrode have similar shapes. The total charge storage mechanism can be separated into three components: the faradaic contribution from the battery process of Li<sup>+</sup> insertion, the surface pseudocapacitance and the non-faradaic processes in the double layer capacitor.<sup>1</sup> All that can be calculated according to the following Equations<sup>2</sup>

$$i(V)=av^b$$

Where  $i(V)$  is the current density,  $v$  is the scan rate, and  $a$  and  $b$  are adjustable parameters. The  $b$  value is determined from the slope of the plot of  $\log i$  versus  $\log v$ , and the charge storage mechanism can be revealed from the  $b$  values. In detail, when  $b \approx 0.5$ , it is dominated by diffusion-controlled process and when  $b \approx 1$ , it is dominated by the capacitive process.<sup>2</sup> Figure S11(b) shows the  $\log i(V)$  versus  $\log v$  plots at different oxidation/reduction peaks; the  $b$ -values are in the range of 0.7–1.0. This indicates that the charge storage is predominantly controlled by the capacitive process, which leads to a fast Li<sup>+</sup> insertion/ extraction. In addition, the current can be expressed more precisely as the sum of the surface-controlled and diffusion-controlled capacities at a fixed potential<sup>3</sup>

$$i(V)=k_1v + k_2v^{1/2}$$

By determining both  $k_1$  and  $k_2$  constants, we can distinguish the fraction of the current from surface capacitance and Li<sup>+</sup> semi-infinite linear diffusion. It is noteworthy that the role of

capacitive contribution of both electrodes further enlarges with the scan rate increases, as shown in Figure S11(c).

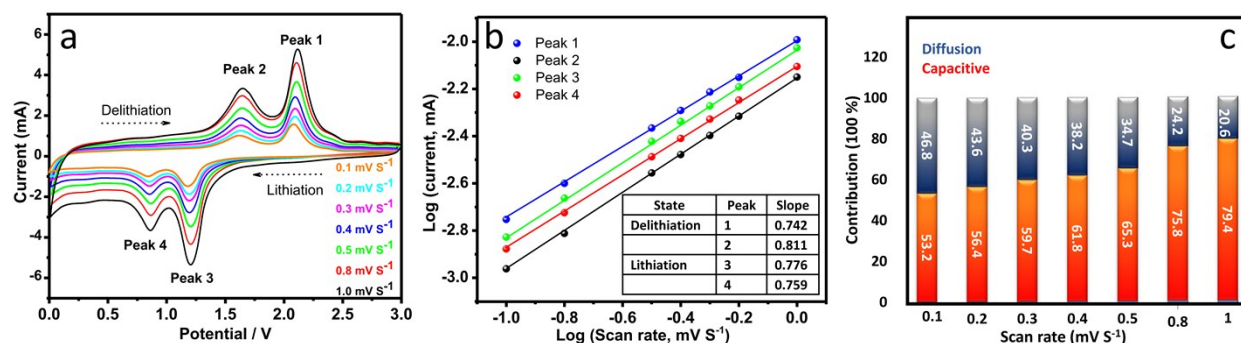


**Figure S10.** (a) CV curves of ZnCoS@Co<sub>9</sub>S<sub>8</sub>/NC electrode at different scan rate ranging from 0.2 to 1 mV S<sup>-1</sup>. (b) Log (i) versus log (v) plots. (c) Contribution ratio of capacitive and diffusion controlled behaviors at various scan rates.

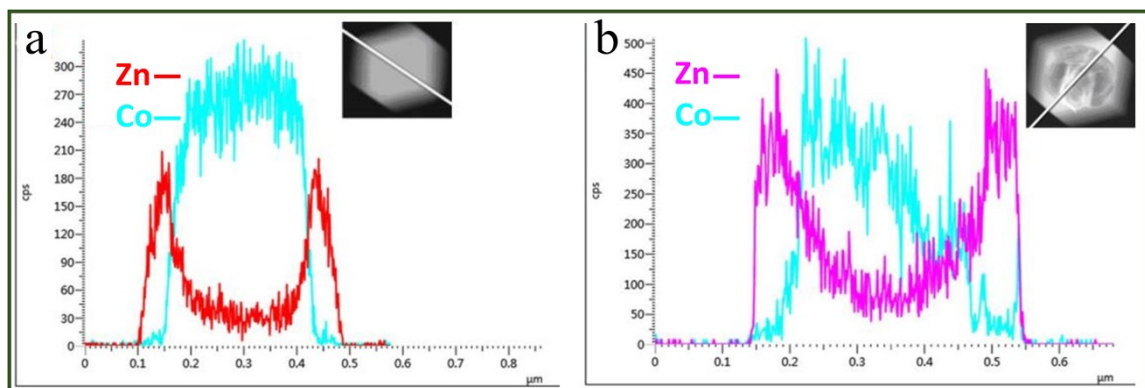


**Figure S11.** Line scan pattern of (a) Zn<sub>50</sub>Co<sub>50</sub>-ZIF and (b) Hollow- ZnCoS-ZIF (after refluxed sulfidation).

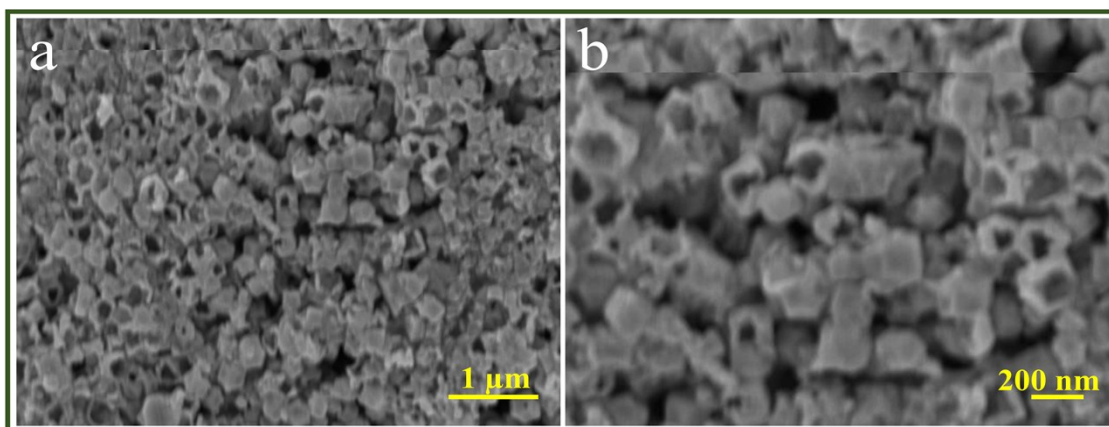
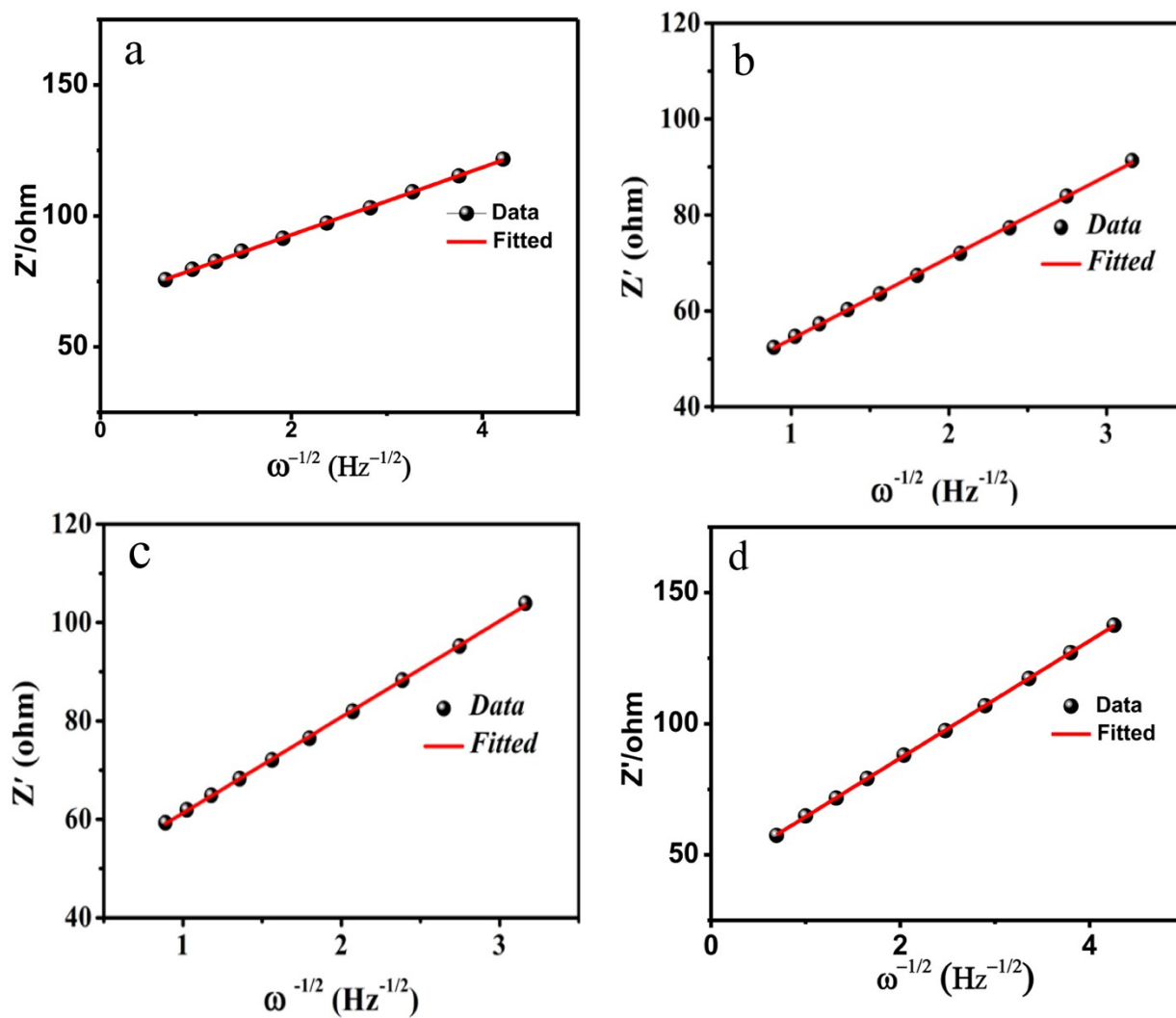
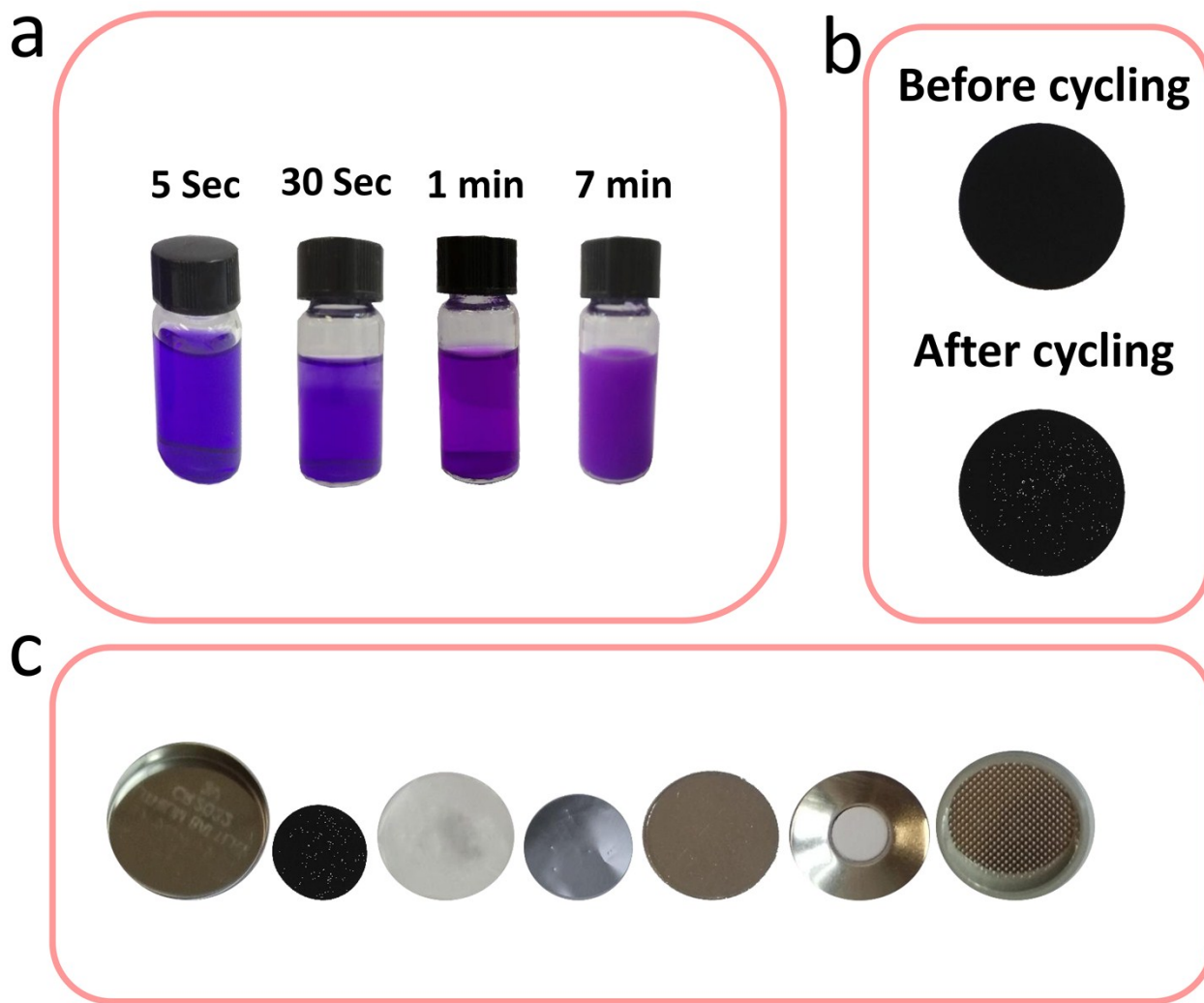


Figure S12. FESEM images of ZnCoS@Co<sub>9</sub>S<sub>8</sub>/NC electrode after 400 charge-discharge cycles.



**Figure S13.** Fitted straight lines of  $Z'$  vs.  $\omega^{-1/2}$  at low frequency region for ZnCoS@Co<sub>9</sub>S<sub>8</sub>/NC(a), ZnCo@Co-NC/NC (b), ZnCoS@CoS/NC (c) and Co<sub>1-x</sub>S@Co<sub>9</sub>S<sub>8</sub>/NC electrodes (d).



**Figure S14.** (a) Photograph of ZIF-67 formation as discussed above in synthesis (a), photograph of working electrodes before and after cycling (b), photograph of parts of coin-type cell after long cycling performance(c).

Figure S13(a) showing that homogeneous solution of 2-mIM and Cobalt nitrate transformed from transparent to turbid over time, in the first 7 min. nucleation occurred and nanocrystals of ZIF-67 are formed and then zinc nitrate solution was added to make ZIF-67/ZIF-8@ZIF-67 as illustrated in Figure S1. Figure S13(b) shows that active material was not peeled

out from current collector after 50 cycles, it could be attributed to the strong contact between current collector and active material slurry.

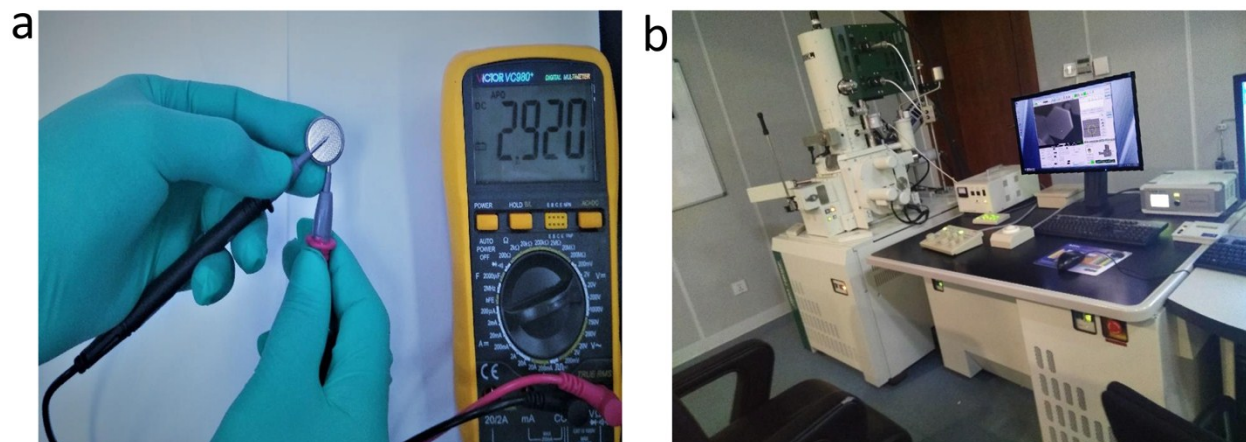


**Fig. S15.** (a) Photograph of voltage measured of freshly prepared coin-type cell, (b) photograph of FESEM measurement at situ.

**Table S1.** Performance comparison of single-holed hollow core-shelled ZnCoS@Co<sub>9</sub>S<sub>8</sub>/NC in this work and the cobalt sulfides-based electrodes reported in literatures.

Materials	Reversible capacity (m Ah g <sup>-1</sup> )	Rate performance (m Ah g <sup>-1</sup> )	Capacity retention (cycling range) (m sssAh g <sup>-1</sup> )	Ref.
CoS <sub>2</sub> /RGO	1499 at 100 mA g <sup>-1</sup>	440 at 2 A g <sup>-1</sup>	1245 (83.1%), (2–150 cycles)	4
MWCNT@a-C@Co <sub>9</sub> S <sub>8</sub>	805 at 1 A g <sup>-1</sup>	646 at 2 A g <sup>-1</sup>	662 (82.2%), (6–120 cycles)	5
rGO/Co <sub>9</sub> S <sub>8</sub> /Co <sub>1-x</sub> S	748 at 200 mA g <sup>-1</sup>	547 at 2 A g <sup>-1</sup>	994 (132.9%), (2–150 cycles)	6
CoS@PCP/CNTs-600	1278 at 200 mA g <sup>-1</sup>	752 at 10 A g <sup>-1</sup>	1668 (130.5%), (2–100 cycles)	7
CoS <sub>2</sub> polyhedron	738 at 100 mA g <sup>-1</sup>	155 at 1 A g <sup>-1</sup>	694 (94.0%), (2–100 cycles)	8

Co <sub>9</sub> S <sub>8</sub> /graphitic carbon	1770 at 100 mA g <sup>-1</sup>	692 at 3 A g <sup>-1</sup>	1600 (90.4%), (2–40 cycles)	9
Co <sub>9</sub> S <sub>8</sub> -650	1040 at 100 mA g <sup>-1</sup>	635 at 2 A g <sup>-1</sup>	1400 (134.6%), (2–100 cycles)	10
CoS <sub>2</sub> /CNT	691 at 200 mA g <sup>-1</sup>	338 at 1 A g <sup>-1</sup>	900 (130.2%), (2–180 cycles)	11
NC/CoS <sub>2</sub> -650	700 at 100 mA g <sup>-1</sup>	340 at 2.5 A g <sup>-1</sup>	560 (80%), (2–50 cycles)	12
C@Co <sub>9</sub> S <sub>8</sub> dandelion	636 at 1 A g <sup>-1</sup>	373 at 6 A g <sup>-1</sup>	520 (81.8%), (2–50 cycles)	13
CoS <sub>2</sub> /graphene	805 at 50 mA g <sup>-1</sup>	360 at 0.8 A g <sup>-1</sup>	630 (78.3%), (2–40 cycles)	14
RGO/Co <sub>9</sub> S <sub>8</sub>	595 at 545 mA g <sup>-1</sup>	534 at 1.1 A g <sup>-1</sup>	382 (64.2%), (2–500 cycles)	15
CoS <sub>2</sub> /graphene	890 at 100 mA g <sup>-1</sup>	641 at 1 A g <sup>-1</sup>	800 (89.9%), (2–150 cycles)	16
Cobalt sulfides/GNS	1018 at 100 mA g <sup>-1</sup>	680 at 1 A g <sup>-1</sup>	954 (93.7%), (2–50 cycles)	17
N-doped carbon@CoS	750 at 2A g <sup>-1</sup>	750 at 4 A g <sup>-1</sup>	671 (89.5%), (2–1400 cycles)	18
Co <sub>9</sub> S <sub>8</sub> @C fibers	1105 at 54 mA g <sup>-1</sup>	318 at 2.7 A g <sup>-1</sup>	872 (78.9%), (2–100 cycles)	19
Co <sub>9</sub> S <sub>8</sub> -coated carbon	637 at 100 mA g <sup>-1</sup>	351 at 1 A g <sup>-1</sup>	540 (84.8%), (2–300 cycles)	20
CoS <sub>2</sub> Hollow sphere	925 at 50 mA g <sup>-1</sup>	—	320 (34.6%), (2–40 cycles)	21
Flower-like Co <sub>1-x</sub> S	928 at 100 mA g <sup>-1</sup>	—	485 (52.6%), (2–150 cycles)	22
CoS/Ni core-branch	672 at 1C	371 at 6C	670 (99.7%), (2–200 cycles)	23

CoS/graphene	1200 at 59 mA g <sup>-1</sup>	391 at 1.77 A g <sup>-1</sup>	898 (74.8%), (2–80 cycles)	24
CoS <sub>2</sub> hollow prisms	867 at 1 A g <sup>-1</sup>	470 at 5 A g <sup>-1</sup>	737 (85.0%), (2–200 cycles)	25
worm-like CoS <sub>2</sub>	1140 at 100 mA g <sup>-1</sup>	501 at 2 A g <sup>-1</sup>	883 (77.5%), (2–100 cycles)	26
NiCo <sub>2</sub> S <sub>4</sub> nanotube	1180 at 140 mA g <sup>-1</sup>	212 at 2.8 A g <sup>-1</sup>	710 (60.2%), (2–50 cycles)	27
<b>single-holed hollow core –shelled ZnCoS@Co<sub>9</sub>S<sub>8</sub>/NC</b>	1285 at 0.5 A g <sup>-1</sup>	418 at 2 A g <sup>-1</sup>	1813 (141%), (3-500 cycles)	<b>Our Work</b>

## References

1. Q. Yun, Q. Lu, X. Zhang, C. Tan and H. Zhang, *Angew. Chem. Int. Ed.*, 2018, **57**, 626-646.
2. Z. Hu, L. Wang, K. Zhang, J. Wang, F. Cheng, Z. Tao and J. Chen, *Angew. Chem.*, 2014, **126**, 13008-13012.
3. D. Chao, C. Zhu, P. Yang, X. Xia, J. Liu, J. Wang, X. Fan, S. V. Saviolov, J. Lin and H. J. Fan, *Nature communications*, 2016, **7**, 12122.
4. F. Fu, Y. Chen, P. Li, J. He, Z. Wang, W. Lin and W. Zhang, *RSC Advances*, 2015, **5**, 71790-71795.
5. Y. Zhou, D. Yan, H. Xu, S. Liu, J. Yang and Y. Qian, *Nanoscale*, 2015, **7**, 3520-3525.
6. Z. Li, W. Li, H. Xue, W. Kang, X. Yang, M. Sun, Y. Tang and C.-S. Lee, *RSC Advances*, 2014, **4**, 37180-37186.
7. R. Wu, D. P. Wang, X. Rui, B. Liu, K. Zhou, A. W. K. Law, Q. Yan, J. Wei and Z. Chen, *Adv. Mater.*, 2015, **27**, 3038-3044.
8. Y. Wang, J. Wu, Y. Tang, X. Lü, C. Yang, M. Qin, F. Huang, X. Li and X. Zhang, *ACS Applied Materials & Interfaces*, 2012, **4**, 4246-4250.
9. J. Liu, C. Wu, D. Xiao, P. Kopold, L. Gu, P. A. van Aken, J. Maier and Y. Yu, *Small*, 2016, **12**, 2354-2364.
10. Y. Zhou, D. Yan, H. Xu, J. Feng, X. Jiang, J. Yue, J. Yang and Y. Qian, *Nano Energy*, 2015, **12**, 528-537.
11. Z. X. Huang, Y. Wang, J. I. Wong, W. H. Shi and H. Y. Yang, *Electrochim. Acta*, 2015, **167**, 388-395.
12. Q. Wang, R. Zou, W. Xia, J. Ma, B. Qiu, A. Mahmood, R. Zhao, Y. Yang, D. Xia and Q. Xu, *Small*, 2015, **11**, 2511-2517.
13. W. Shi, J. Zhu, X. Rui, X. Cao, C. Chen, H. Zhang, H. H. Hng and Q. Yan, *ACS Applied Materials & Interfaces*, 2012, **4**, 2999-3006.
14. J. Xie, S. Liu, G. Cao, T. Zhu and X. Zhao, *Nano Energy*, 2013, **2**, 49-56.

15. H. Wang, S. Lu, Y. Chen, L. Han, J. Zhou, X. Wu and W. Qin, *Journal of Materials Chemistry A*, 2015, **3**, 23677-23683.
16. J. Guo, F. Li, Y. Sun, X. Zhang and L. Tang, *Electrochim. Acta*, 2015, **167**, 32-38.
17. G. Huang, T. Chen, Z. Wang, K. Chang and W. Chen, *J. Power Sources*, 2013, **235**, 122-128.
18. Y. Chen, X. Li, K. Park, L. Zhou, H. Huang, Y.-W. Mai and J. B. Goodenough, *Angew. Chem. Int. Ed.*, 2016, **55**, 15831-15834.
19. G. Qu, H. Geng, D. Ge, M. Tang, J. Zheng and H. Gu, *Electrochim. Acta*, 2016, **211**, 305-312.
20. X. Meng and D. Deng, *Chem. Mater.*, 2016, **28**, 3897-3904.
21. Q. Wang, L. Jiao, Y. Han, H. Du, W. Peng, Q. Huan, D. Song, Y. Si, Y. Wang and H. Yuan, *The Journal of Physical Chemistry C*, 2011, **115**, 8300-8304.
22. S. Liu, J. Wang, J. Wang, F. Zhang, F. Liang and L. Wang, *CrystEngComm*, 2014, **16**, 814-819.
23. M. Chen, J. Zhang, X. Xia, M. Qi, J. Yin and Q. Chen, *Electrochim. Acta*, 2016, **195**, 184-191.
24. S. Kong, Z. Jin, H. Liu and Y. Wang, *The Journal of Physical Chemistry C*, 2014, **118**, 25355-25364.
25. L. Yu, J. F. Yang and X. W. Lou, *Angew. Chem. Int. Ed.*, 2016, **55**, 13422-13426.
26. R. Jin, L. Yang, G. Li and G. Chen, *Journal of Materials Chemistry A*, 2015, **3**, 10677-10680.
27. D. J. Yu, Y. F. Yuan, D. Zhang, S. M. Yin, J. X. Lin, Z. Rong, J. L. Yang, Y. B. Chen and S. Y. Guo, *Electrochim. Acta*, 2016, **198**, 280-286.